DOI: 10.1039/C4RA01468E

RSC Advances

PAPER

View Article Online
View Journal | View Issue

Cite this: *RSC Adv.*, 2014, **4**, 29612

Poly(dimethylsiloxane) as a pre-coating in layer-by-layer films containing phosphotungstate nanoclusters electrochemically sensitive toward *s*-triazines†

A. L. Souza,*[a] G. Tremiliosi Filho,[a] L. T. Kubota,[b] R. K. Mendes,[c] A. M. Botelho do Rego,[d] O. N. Oliveira, Jr,[e] C. Henry de Villeneuve,[f] J. N. Chazalviel,[f] P. Allongue,[f] F. Ozanam[f] and U. P. Rodrigues Filho[a]

Received 19th February 2014
Accepted 23rd June 2014

DOI: 10.1039/c4ra01468e

www.rsc.org/advances

One of the major advantages of the Layer-by-Layer (LbL) deposition technique is the possible control of molecular architecture, not only to achieve optimized properties but also to seek synergy among different materials. In this study, LbL films containing nanoclusters of a Keggin type polyoxometalate, phosphotungstic acid (HPW), alternated with the polycation poly(allylamine hydrochloride) (PAH) were deposited on indium-tin oxide (ITO) substrates. The electrochemical properties of the hybrid LbL film investigated in acidic conditions indicated no significant desorption of HPW, when a layer of poly(dimethylsiloxane) terminated with 3-aminopropyl groups (PDMS) was previously deposited on the ITO substrate. Such effect occurred because PDMS prevents desorption of HPW from the hybrid film, as shown by X-ray Photoelectron Spectroscopy (XPS) analyses. The porous structures of the films were revealed by Fourier transform infrared reflection absorption spectroscopy, scanning electron microscopy and XPS. PDMS/PAH as a pre-coating allowed the HPW/PAH films to be sensitive to the electrochemical detection of the triazines atrazine and melamine. In conclusion, the precise control of the LbL films architecture is important to develop opportunities for new applications.

A Introduction

The electrostatic layer-by-layer (LbL) technique has been increasingly used to produce films with controlled architectures, with the advantage of simplicity and versatility.[1] It was primarily conceived for adsorption of layers of oppositely charged polyelectrolytes, but films have been obtained upon exploiting other interactions, including hydrogen bonding,[2] charge-transfer,[3] covalent bonds[4] and biospecific interactions.[5] A number of materials are now used, stemming from polyelectrolytes[6] to metal complexes,[7] metal nanoparticles,[8] metal-oxide clusters[9–11] and biomolecules,[12] for an equally wide variety of applications, including sensors,[13] biosensors[14,15] and electro- and photochromic devices.[16] Of particular relevance for the present work are the polyoxometalate clusters (POMs), which are nanosized metal-oxide clusters also used in LbL films.[9] Their different shapes and sizes make them attractive for applications in electro-optical devices, sensors and anti-corrosion coatings.[17] These compounds may undergo multiple reversible electron transfer reactions without losing their structure,[18] being therefore useful for catalysis,[19] electrocatalysis[20] and electro- or photochromic devices.[21–23] The incorporation of polyoxometalate clusters in films is advantageous in the construction of nanostructures,[24] since systems may be obtained with controlled architectures and useful magnetic, catalytic, photoluminescent, electro- and photochromic properties.[25] POMs are suitable for the LbL technique because of their solubility in aqueous solutions and high anionic charge. LbL films from POMs have been produced with alternating layers of cationic metal complexes,[26–28] metal nanoparticles[29–32] and polymers such as poly(allylamine hydrochloride), poly(ethyleneimine), chitosan and poly(amidoamine).[33–36] For sensing purposes, the most common application, POMs LbL films were deposited onto gold

[a]*Instituto de Química de São Carlos, Universidade de São Paulo, Av. Trabalhador São-carlense, 400, P.O. Box 780, CEP 13566-560, São Carlos, SP, Brazil. E-mail: adriano_lsouza@hotmail.com*

[b]*Instituto de Química, UNICAMP, P.O. Box 6154, CEP 13083-862, Campinas, SP, Brazil*

[c]*Pontifical Catholic University of Campinas, Faculty of Chemistry, 13012-970, Campinas, SP, Brazil*

[d]*Centro de Química-Física Molecular and Institute of Nanoscience and Nanotechnology, Instituto Superior Técnico, Technical University of Lisbon, 1049-001, Lisboa, Portugal*

[e]*Instituto de Física de São Carlos, Universidade de São Paulo, Av. Trabalhador São-carlense, 400, P.O. Box 780, CEP 13566-560, São Carlos, SP, Brazil*

[f]*Physique de La Matière Condensée, École Polytechnique, CNRS, Palaiseau, France*

† Electronic supplementary information (ESI) available. See DOI: 10.1039/c4ra01468e

electrodes, glassy carbon and glass coated with indium tin oxide (ITO).[34,37,38] The analytes detected included nitrite, bromate, iodate, arsenite, oxalate, hydrogen peroxide and NO.[26–29,34,37–44]

In this paper, we report on the electrochemical properties of LbL films containing a Keggin-type POM, the phosphotungstic acid (HPW), deposited onto ITO. Particular emphasis is given to the effect of the PDMS aminopropyl terminated pre-coating layer on the electrochemical response of the LbL films. This architecture showed the best electrochemical behavior and was characterized by UV-vis absorption spectroscopy, absorption–reflection infra-red spectroscopy (FT-IRRAS), X-ray photoelectron spectroscopy (XPS) and surface plasmon resonance. The film with optimized architecture was then tested in terms of sensitivity against melamine and atrazine, compounds presenting the symmetric triazine ring. It is the first time that films with Keggin polyoxometalates are used for electrooxidation of triazines. The motivation to study electrooxidation of melamine arose from its use in adhesives and plastics, in addition to its having become known worldwide with the death of children owing to contaminated milk in China in the last decade.[45] In respect to atrazine, it is often used as pesticide and may cause contamination of soil and waterways.[46] Therefore, the study of the electrocatalytic activity of these films bearing phosphotungstates can be useful in the design of new electrochemical sensors for these molecules; so far only modified electrodes based on molecularly imprinted polymers have been used for this purpose.[47,48]

B Experimental section

B.1 Chemicals

Phosphotungstic acid (HPW), poly(allylamine)hydrochloride (PAH), (3-aminopropyl)triethoxysilane (APTS), poly(dimethylsiloxane)bis (3-aminopropyl) terminated (PDMS), isopropyl alcohol, chitosan (medium molecular weight), melamine, atrazine (Pestanal) and potassium hexacyanoferrate(III) were purchased from Sigma-Aldrich. Potassium hexacyanoferrate(II) and potassium chloride were purchased from Mallinckrodt. Indium tin oxide (ITO)-coated glass with a resistance $\leq 10\ \Omega$ was acquired from Delta Technologies. Ultrapure deionized water with a resistivity of 18.2 MΩ cm was supplied by a Millipore system. Perchloric acid and sodium perchlorate were purchased from Vetec. Ammonium hydroxide, hydrogen peroxide, acetone, acetic acid and sulfuric acid were obtained from Synth. Commercial grade nitrogen gas was purchased from AGA.

B.2 Layer-by-Layer (LbL) Films

Electrostatic LbL films were prepared by immersion of the pre-coated substrate, as described hereafter, in aqueous solutions of HPW and PAH alternately. The concentrations of HPW and PAH solutions were 5.0×10^{-4} mol L^{-1} and 1.0×10^{-3} mol L^{-1} respectively, with pH = 1.0 (in $HClO_4$ medium). The pre-coated substrate was immersed in HPW solution for 10 min, washed in a $HClO_4$ solution (pH = 1.0) for 30 s and dried with a nitrogen stream. Then it was immersed in PAH solution for 10 min with the washing and drying procedures being repeated as for the HPW layer. At this stage, one bilayer of HPW/PAH was formed. The procedure was repeated for obtaining the desired number of bilayers. ITO and quartz substrates were cleaned using the RCA procedure.[49] The slides were immersed in a solution of H_2O–H_2O_2–NH_4OH in a 5 : 1 : 1 (v/v/v) proportion for 30 min at 80 °C, after which they were rinsed with deionized water and dried with a stream of nitrogen gas. Four pre-coatings of the substrates were performed before the adsorption of (HPW/PAH) bilayers:

(i) Pre-coating PAH: a layer of PAH was preadsorbed from the aqueous solution for 10 min, washed in a $HClO_4$ solution (pH = 1.0) for 30 s and dried with a nitrogen stream.

(ii) Pre-coating (PDMS/PAH): a layer of poly(dimethylsiloxane)-bis(3-aminopropyl) terminated (PDMS) was pre adsorbed for 30 min from an isopropyl alcohol solution with a PDMS concentration of 0.50 g L^{-1} followed by the adsorption of a PAH layer as in (i).

(iii) Pre-coating APTS: a layer of (3-aminopropyl)triethoxysilane (APTS) was preadsorbed by immersion into an APTS 0.1% (v/v) solution in acetone for 50 min.

(iv) Pre-coating chitosan: a layer of chitosan was preadsorbed from a 0.50 g L^{-1} aqueous solution of acetic acid 2%.

B.3 Electrochemical Measurements

The LbL films deposited onto ITO substrates had their electrochemical properties studied with a potentiostat PGSTAT30 AutoLab, Ecochemie. Cyclic voltammetry and differential pulse voltammetry (DPV) were performed using a 3-electrode electrochemical cell, where the working electrode was the modified ITO substrate, the saturated calomel electrode (SCE) was used as reference, and the counter electrode was a platinum wire. The supporting electrolyte was an aqueous solution of 0.10 mol L^{-1} $HClO_4$. Solutions of melamine and atrazine were prepared and used immediately also in 0.10 mol L^{-1} $HClO_4$. The areas of the ITO electrodes were estimated by cyclic voltammetry experiments in an aqueous solution of 6.0×10^{-3} mol L^{-1} potassium hexacyanoferrate(II) in 0.10 mol L^{-1} KCl, using the Randles–Sevcik equation.[50] All the electrochemical measurements were made at room temperature with the electrolyte solution being deaerated with nitrogen gas for at least 20 min. During the experiments, the electrolyte was kept under a nitrogen atmosphere.

B.4 Spectroscopic and microscopic characterizations

The XPS measurements were performed with a XSAM spectrometer (KRATOS) in the fixed transmission mode with pass-energy of 20 eV and non-monochromatized radiation (line MgKα at 1253.6 eV or AlKα at 1486.6 eV). The power of the source was 120 W (12 kV × 10 mA). The measurements were carried out in ultra-high vacuum at 10^{-7} Pa. Spectra were fitted with pseudo-Voigt profiles (weighted products of Gaussian and Lorentzian profiles) using the non-linear least square fitting method in the XPSPEAK41 package. Correction of binding energies (BE) due to charge accumulation was made assigning the C 1s lowest BE fitted peak to sp^3 (*i.e.* carbon bound just to carbon and hydrogen) a BE = 285 eV.[51]

The absorption–reflection Fourier transform infrared spectra (FT-IRRAS) were acquired in a BOMEM MB-100 and a Bruker EQUINOX spectrometers. One hundred interferometer sweeps were averaged for each spectrum to a resolution of 4 cm^{-1}. A homemade ATR chamber including a rotatable grid polarizer on the IR beam was used. The substrates were Ge(111) trapezoidal blocks 2.5 cm long, 0.5 mm thick, and 45° bevelled edges, which had been cleaned with several immersions into sulfochromic solution (mixture of $Na_2Cr_2O_7$ and sulfuric acid) for 5 min and into an aqueous HF 5% solution for 10 s. The UV-visible spectra were obtained with a Jasco spectrophotometer, while Surface Plasmon Resonance (SPR) experiments were carried out with an AutoLab apparatus from Eco Chemie with 670 nm incident light. The substrate for the adsorption was a gold disk. It was cleaned by immersion in a 3 : 1 (v/v) H_2SO_4–H_2O_2 solution ("Piranha solution") for 5 min, and then washed with copious amounts of deionized water and dried with a nitrogen gas stream. Morphological studies with scanning electron microscopy with a field emission gun (FEG-SEM) were carried out using a Hitachi S-4800 Field-Emission-Gun SEM.

C Results and discussion

C.1 Effect of the ITO pre-coating in LbL films with HPW

Fig. 1 compares cyclic voltammograms (CVs) for successive potential cycles for 5-bilayers (HPW/PAH) LbL films deposited on ITO pre-coated with PAH and PDMS/PAH. At the pre coated ITO/PAH electrode the two redox processes are around 0 and −0.25 V. At the ITO/PDMS/PAH electrode the corresponding redox waves are shifted by *ca.* 50 mV toward more negative potentials. In addition, the potential difference (ΔE_p) measured between the anodic and cathodic peaks of a given redox reaction is a little larger for this electrode. These features could be related to the electrical insulating role of PDMS. Nevertheless, after 100 potential cycles the two types of films exhibited similar CVs irrespectively of the pre coatings.

To interpret the CVs in Fig. 1, we briefly recall past studies about the electrochemical behavior of HPW in solution. Using potentiometric titration and polarography, Pope and Varga[52] showed that HPW in acidic medium (H_2SO_4 1 mol L^{-1}) exhibits reduction waves at −0.023 V and −0.275 V *vs.* SCE, assigned to two reduction processes involving one electron in each process. Keita and Nadjo[53] observed 5 reduction waves for HPW in $HClO_4$ 1 mol L^{-1} medium. The first three ones at −0.02 V, −0.257 V and −0.59 V *vs.* SCE, were ascribed to reduction processes involving one, one and two electrons, respectively. The other two reduction waves at −0.775 V and −0.85 V *vs.* SCE, involved more than two electrons, though the precise number was not determined. In this latter study,[53] the working electrode was a glassy carbon electrode and the counter electrode was platinum gauze with large surface area.

Based on these results, it is tempting to identify our waves at 0 and −0.25 V with the first ($[PW_{12}O_{40}]^{3-} \rightarrow [PW_{12}O_{40}]^{4-}$) and second ($[PW_{12}O_{40}]^{4-} \rightarrow [PW_{12}O_{40}]^{5-}$) reduction steps of the HPW, respectively. However, the wave around 0 V appears surprisingly small. This is based on the assumption that the phosphotungstate species are well dispersed and immobile within the film.

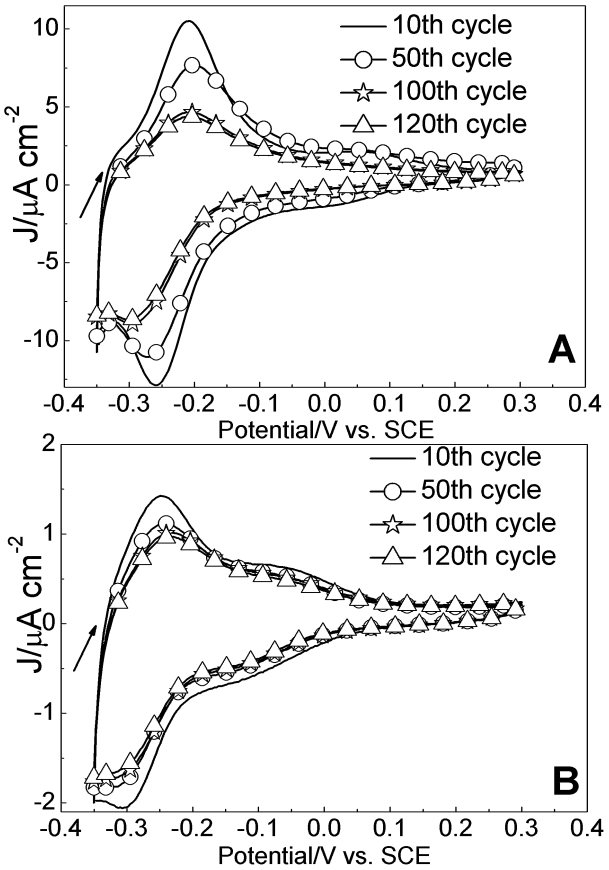

Fig. 1 Cyclic voltammograms for modified ITO substrates with 5-bilayers (HPW/PAH) LbL films for various potential cycling. ITO pre-coatings were (A) PAH and (B) PDMS/PAH. The supporting electrolyte was an aqueous solution of 0.10 mol L^{-1} $HClO_4$ (pH = 1.0). Scan rate: 20 mV s^{-1}.

Under this hypothesis, electron transfer to the ITO substrate requires electron hopping between HPW centers. This process is expected to electric field dependent and therefore be slower for the more positive redox wave than for the one at −0.25 V. As a result, the wave around 0 V (assigned to ($[PW_{12}O_{40}]^{3-} \rightarrow [PW_{12}O_{40}]^{4-}$) essentially concerns those HPW species located close to the surface while the wave around −0.25 V (assigned to $[PW_{12}O_{40}]^{4-} \rightarrow [PW_{12}O_{40}]^{5-}$) involves HPW centers distributed deeper within the film. As a result, the 0 V wave should have a smaller area, as observed, thus explaining the area discrepancy between the waves at −0.25 V and 0 V *vs.* SCE. The permeability of the films pre-coated with PAH and PDMS/PAH with respect to $[Fe(CN)_6]^{4-}$ ion is exhibited in Fig. S1 of the ESI.†

To compare the influence of the pre-coating on the electrochemical behaviour of 5-bilayers (HPW/PAH) LbL films, we measured the anodic charge in CVs. They were calculated from the sum of the areas of the two anodic waves in the CV for a given film. These areas extracted from CVs were obtained for at least three films freshly prepared. Fig. 2 shows that this charge density always decreases with increasing number of potential

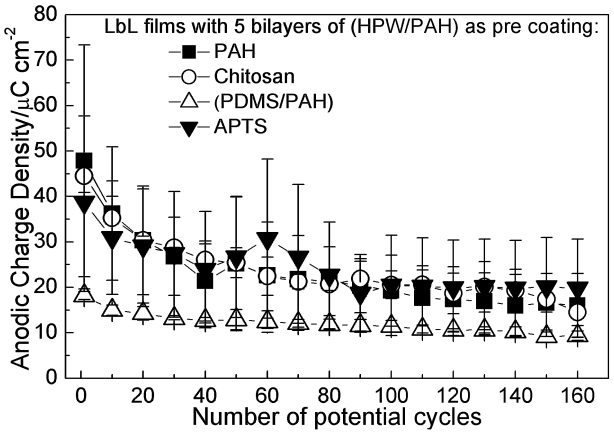

Fig. 2 Anodic charge densities for modified ITO substrates with 5-bilayers (HPW/PAH) LbL films with different ITO pre-coatings tested. They were extracted from the CVs in an aqueous solution of $HClO_4$ at pH = 1.0 as supporting electrolyte and using a scan rate of 20 mV s^{-1}.

cycles. For the PAH or APTS pre coatings, the reproducibility was poor because the standard deviation values are very high. With chitosan as pre-coating, the electrochemical response was not stable either in Fig. S2 in the ESI.† Despite its lower initial charge density, the film on PDMS/PAH had the smallest loss in charge density, thus appearing as better architecture for the 5-bilayers (HPW/PAH) LbL films. Indeed, there was a decrease in the current density up to the 50th cycle, with a drop of 25–30% between the 10th and 100th cycles. This drop in current intensity is consistent with the result for multilayers of $[SiW_{12}O_{40}]^{4-}$ electrodeposited with 4-poly(vinylpyridine) on a gold electrode.[37]

The loss of electrochemical response may be related to the egression of the $[PW_{12}O_{40}]^{3-}$ into the solution or to an increase in ITO film resistivity due to its progressive corrosion. For all films studied here, there is a desorption of In^{3+} from the ITO electrode due to the chemical dissolution (corrosion) in the acidic condition used, which results in LbL disjointing and an increase of resistivity of the electrode. Furthermore, an HPW desorption also occurs but at minor extent for PDMS/PAH pre-coated electrodes. Stotter *et al.*[54] noted increased resistivity and roughness for ITO owing to dissolution after treatment in acidic or basic conditions. Similar conclusions were found by Senthilkumar *et al.*,[55] where the changes on the ITO surface occurred when the electrodes were submitted to potential cycling from 0.2 to −1.0 V *vs.* SCE at pH = 2.2 and 4.2. Under more acidic conditions, the ITO resistance increased with the appearance of dark spots on its surface, owing to corrosion. This also caused loss in optical transmittance. These effects were verified in potential cycles from 0.2 to −1.2 V *vs.* SCE. An analysis of the Pourbaix diagrams for In_2O_3 (ref. 56) and SnO_2 (ref. 57) oxides leads to the same conclusions. For instance, evidence for ITO corrosion/dissolution to In^{3+} was noted in the In_2O_3 Pourbaix diagram for pH = 1.0, regardless of the potential range. For SnO_2, the Pourbaix diagram exhibits a similar tendency for this pH, with the possible formation of metallic tin at more negative potential values.

The use of highly acidic conditions in this paper is justified because decomposition of HPW occurs at pH > 1.5, where the formation of lacunary structures occurs.[58] In the layers of (HPW/PAH) deposited onto (PDMS/PAH) layers, PDMS acts in preventing HPW desorption. Further evidence for this conclusion will be given with XPS data. Tests with a larger number of (HPW/PAH) bilayers were not carried out, because the HPW electrochemical response did not increase significantly above 10 bilayers, and the redox pairs are not as well defined as for films on (PDMS/PAH) (results not shown). We therefore conclude that the 5-bilayers of (HPW/PAH) on (PDMS/PAH) exhibits better electrochemical response than the other films, with a lower loss of current density and a higher reproducibility. This type of film was thus selected for further characterization, as discussed later.

C.2 Characterization of (HPW/PAH) LbL films pre-coated with PDMS/PAH

C.2.1 UV-visible spectroscopy. The UV-visible spectra for the (HPW/PAH) LbL films exhibit a peak at 268 nm, as shown in Fig. 3, which corresponds to a metal-ligand charge transfer observed at 265 nm for HPW in an acidic solution.[18] The inset shows the absorbance at the peak increasing linearly after the 3rd bilayer.

C.2.2 (FT-IRRAS) study. Fig. S3 in the ESI† describes the adsorption time of PDMS on GeO_x/Ge(111) substrate. Fig. 4 displays the FT-IRRA spectra for each deposition stage on PDMS layer in GeO_x/Ge(111) substrate. The disappearance of the symmetric deformation (δ_{sym}) Si–CH_3 band at 1259 cm^{-1} suggests that PDMS molecules diffuse to the solution–film interface, followed by redeposition atop the PAH layer. More details can be found in Fig. S4 in the ESI.† The bands between 1450–1700 cm^{-1} are ascribed to protonated PAH and those between 800 and 1100 cm^{-1} are due to P–O, W=O and W–O–W groups of HPW, respectively. The band broadening is caused by the strong interaction between the PAH ammonium groups and the phosphotungstates.

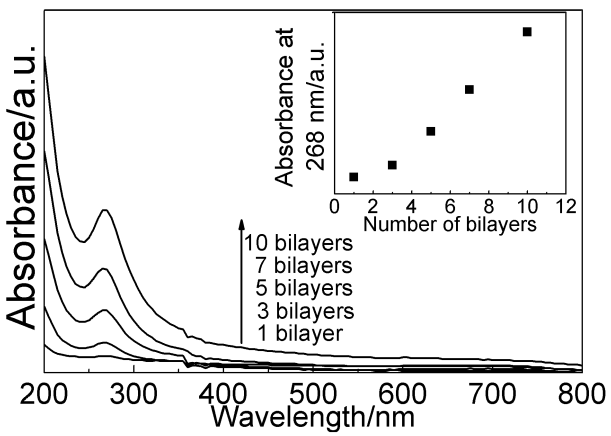

Fig. 3 Electronic spectra in the UV-visible region showing the growth of (HPW/PAH) bilayers on a quartz slide substrate pre-coated with PDMS/PAH. The inset shows the intensity of the band at 268 nm *versus* number of bilayers.

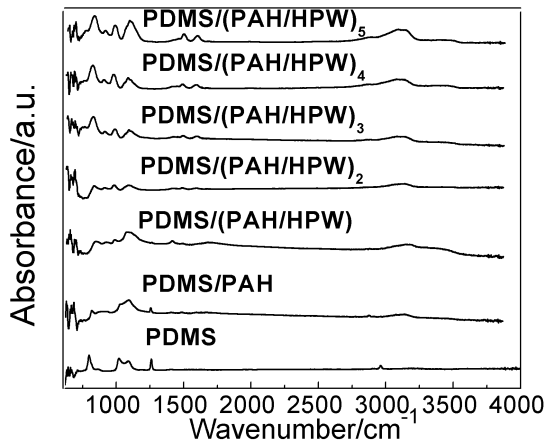

Fig. 4 FT-IRRA spectra at each deposition stage on a GeO_x/Ge(111) substrate. The disappearance of the δ_{sym} Si–CH_3 band at 1259 cm^{-1} is evident.

Surface plasmon resonance was used to study the adsorption kinetics of PAH on PDMS and of HPW on PDMS/PAH films. The gold disk used was previously modified with PDMS as described in the Experimental section. Adsorption of a complete layer of PAH on PDMS took *ca.* 140 s, while the adsorption time for HPW on this PAH layer took 73 s (see Fig. S5 in ESI†).

C.2.3 Surface morphology studied by FEG-SEM experiments. Fig. 5 shows FEG-SEM images for two hybrid films with pre coated layer of PDMS/PAH and PAH. They indicate a clear difference in morphology. When (HPW/PAH) bilayers are deposited onto ITO pre-coated with PDMS/PAH one notes that the film exhibits large, irregular pores, with a topography similar to that of the bare ITO substrate. The latter finding was confirmed with atomic force microscopy (AFM) images taken in the contact mode (see Fig. S6 in ESI†). Therefore, the PDMS layer is sufficiently thin to follow the topography of ITO and makes the film more uniform than for the film without PDMS in the pre-coating layers.

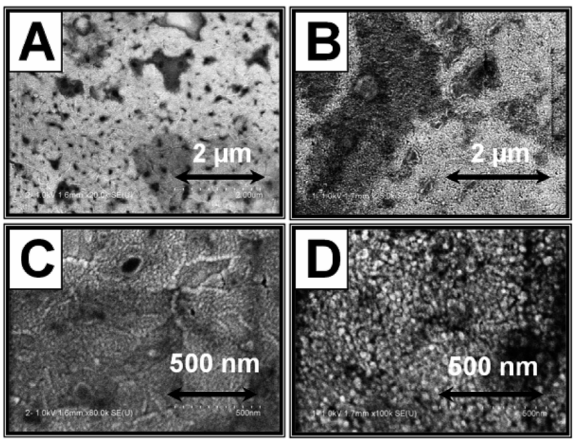

Fig. 5 FEG-SEM images for 5-bilayers (HPW/PAH) LbL films prepared on ITO substrates pre-coated with: (PDMS/PAH) in (A) and (C); PAH in (B) and (D).

The different morphologies of the pre coated PAH and (PDMS/PAH) hybrid films may explain the differences in electrochemical behaviors. From the FT-IRRAS data we inferred that PDMS was partially desorbed and readsorbed forming an overlayer on the film. Such a continuous redeposition would result in a rougher surface as shown in Fig. S7.† When PDMS is absent, the film also results in porous layers due to packing of the globules. The pores formed would allow diffusion of the electrolytes and electroactive species, which explains the electrochemical behaviour of the films with ferrocyanide shown in the ESI.† However, this does not explain the broader peaks and larger ΔE_p for the (PDMS/PAH) based film. In order to solve this question, we resorted to a surface sensitive technique, namely XPS, with a comparison of (HPW/PAH) layers deposited onto ITO pre-coated either with (PDMS/PAH) or just PAH.

C.2.4 XPS. The wide-scan XP spectra for LbL films with 5 bilayers of (HPW/PAH) on ITO/PDMS/PAH and on ITO/PAH are shown in the ESI (Fig. S8†). The presence of HPW is confirmed by the W 4f peaks, while the polymeric species contribute with C 1s and N 1s peaks (PAH) and Si 2p (PDMS). The presence of the latter peak is especially important since XPS is surface sensitive with a probing depth limited to a few monolayers, as determined by the photoelectrons mean free path.[51] Therefore, PDMS is present on the surface, as already inferred from SEM and FT-IRRAS experiments. Another important feature is the presence of In 3d peaks in the wide XP spectra, indicating surface segregation of In from the ITO electrode, as will be discussed later on.

Using for charge correction the first peak of C 1s as being the C–H functional group, the W $4f_{7/2}$ binding energy (BE) was 36.6 ± 0.2 eV for the as-prepared samples and 36.1 ± 0.2 eV after potential cycling as shown in Fig. 6A and B, respectively, for the hybrid film with 5 bilayers of (HPW/PAH) pre coated with PDMS/PAH. Similar spectra for the hybrid film pre coated with PAH can be seen in Fig. S9 in the ESI.† Considering the experimental error, BE seems to decrease after the decrease in potential. The spin–orbit splitting is the same for all the samples, *viz.* 2.1 ± 0.1 eV. Generally, the W 4f spectrum of bulk HPW shows W $4f_{7/2}$ at 35.8 eV (ref. 59) and crystalline HPW displays W $4f_{7/2}$ at 36.1 ± 0.23 eV.[60] Zhang *et al.*[61] obtained 36.5 eV for W $4f_{7/2}$ BE in HPW adsorbed on palygorskite modified with 3-aminopropyltriethoxysilane and *N*-(2-aminoethyl)-3-aminopropyltrimethoxysilane. The increase in W $4f_{7/2}$ BE was attributed to the change from W=O to W–O– binding due to the attachment of surface $–NH_2$ or –NH– groups, probably with hydrogen bonding in W–O···H–N-silane-palygorskite. It is therefore possible to conclude that in the films studied here, HPW would be less strongly adsorbed after the potential cycling, which is consistent with the hypothesized charge transport mechanism. During the potential cycling, HPW diffuses along the film and/or to the bulk solution causing a decrease in the anodic charge density.

The amount of phosphorus in the samples with PDMS/PAH as pre-coating layers is extremely small, which impairs an accurate measurement of the XPS peak areas. Changes in the P 2p BE with cycling cannot be measured since the P 2p signal for the as-prepared samples is too low for a fitting procedure. For

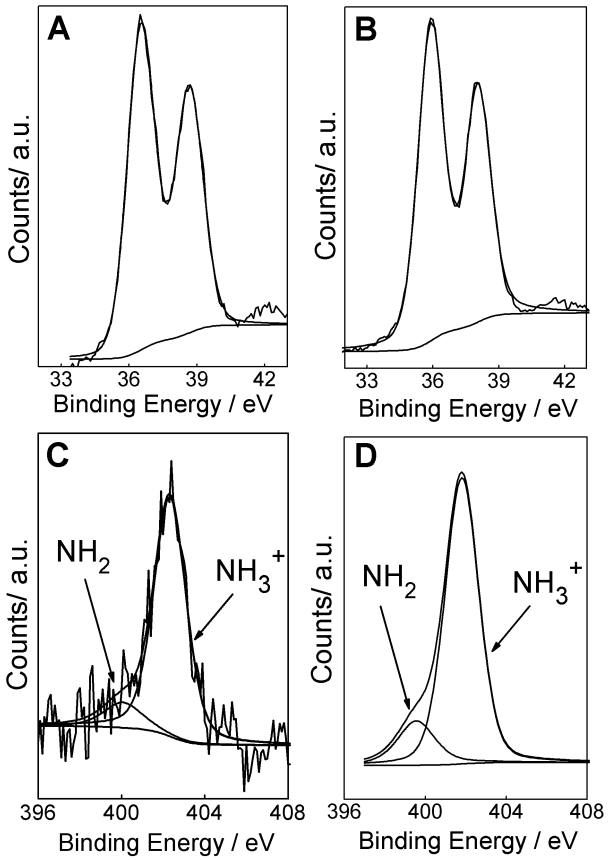

Fig. 6 High resolution XP spectra for ITO modified with 5 bilayers of (HPW/PAH) pre coated with PDMS/PAH. W $4f_{7/2}$ region for as prepared film (A), W $4f_{7/2}$ region after potential cycling (B), N 1s region for as prepared film (C), N 1s region after potential cycling (D).

Table 1 XPS atomic ratios for 5-bilayers (HPW/PAH) LbL films on ITO pre-coated with (PDMS/PAH) and PAH before the potential cycling for two different TOA. * The amount of Sn, being very small, impairs its quantification

Pre-coating	PDMS/PAH		PAH	
TOA	90°	30°	90°	30°
C/In	152	443	23.1	24.7
N/In	5.0	13.1	1.4	1.3
W/In	5.3	7.0	1.7	1.9
Si/In	36.0	56.8	—	—
C/Si	4.1	7.6	—	—
N/Si	0.14	0.23	—	—
W/Si	0.15	0.12	—	—
In/Sn	6.4	*	6.5	6.3
N^+/N	7.9	0.9	3.3	0.6
W/N_{total}	1.3	0.6	1.2	1.4

Table 2 XPS atomic ratios for 5-bilayers (HPW/PAH) LbL films on ITO pre-coated with (PDMS/PAH) and PAH after the potential cycling for two different TOA

Pre-coating	PDMS/PAH		PAH	
TOA	90°	30°	90°	30°
C/In	56	184	303	312
N/In	11.0	20.4	23.9	25.7
W/In	6.0	10.2	11.4	16.0
Si/In	1.5	10.7	—	—
C/Si	37.0	16.8	—	—
N/Si	7.5	1.9	—	—
W/Si	4.0	1.0	—	—
In/Sn	2.8	1.9	3.6	4.8
N^+/N	7.3	4.3	3.5	4.2
W/N_{total}	0.6	0.5	0.5	0.6

the samples without PDMS, the P $2p_{3/2}$ BE decreased from 134.3 ± 0.2 eV in the as-deposited samples to 133.7 ± 0.2 eV in the cycled samples. Values for the P 2p BE in tungstic acid or tungstates are hard to find in the literature probably due to the low P/W ratio. Zhang *et al.*[61] reported 134 eV for P $2p_{3/2}$ BE of $H_3PW_{12}O_{40}$ immobilized on a palygorskite surface modified with aminosilanes, while for several phosphates the values reported range from 133.2 to 134.0 eV.[62] Therefore, the P 2p BE and W 4f BE values obtained here indicate partial decomposition of HPW. This causes loss in electrochemical activity and peak broadening in the voltammogram after potential cycling. Even for this film and using the same reference for the correction of binding energies, the In $3d_{5/2}$ BE was 444.9 ± 0.2 eV for cycled samples and 445.9 ± 0.2 eV for as-prepared samples. These binding energies correspond to In^{3+} in amorphous indium oxide and amorphous indium hydroxide, respectively.[63]

The quantitative analysis in Tables 1 and 2 reinforces the explanation for the change in BE: the W/N ratios decreased with cycling for all the samples. Hence, the HPW should become less bound to PAH, with molecules from the surface diffusing toward the solution with potential cycling.

For the film with 5 bilayers of (HPW/PAH) containing PDMS/PAH as pre-coating, the quantitative analysis at take-off angles (TOA) of 90° (deeper analysis) and 30° (shallower analysis) relative to the sample surface reveals that in the as-prepared film, all the atomic ratios X/In with X = C, N, W and Si, increase when TOA changes from 90° to 30° denoting that both the bilayer film and the pre-coating layers are on top of the ITO. No evidence for In^{3+} mixing with the film during its building was observed. However, when the X/Si atomic ratios are analysed, they increase for TOA = 30° when X = C or N but they decrease when X = W. This is compatible with the PDMS layer mixing with the (HPW/PAH) film but not crossing the shallower PAH layer. These results show that even for the as-prepared film, the PDMS layer was already mixed with the film in agreement with FTIRRAS measurements which showed a decrease in the intensity of the $\delta_{sym}(Si–CH_3)$ band as a function of the number of deposited (HPW/PAH) bilayers.

After cycling, all the ratios X/In are larger than before cycling but keep increasing for TOA = 30°. This strongly suggests that some loss of In occurs due to its diffusion into the solution, pointing to corrosion.

However, a rearrangement of the film, further covering the substrate, could have the same effect. Since the BE values for the

$3d_{5/2}$ photoelectrons are very close for In (445–446 eV) and Sn (486.9–487.4 eV) the In/Sn atomic ratio may be used to clarify this question. The ratio should not be altered by a film rearrangement because the attenuation of both photoelectrons should be similar. However, the ratio should decrease if In loss occurs and decrease from TOA = 90° to TOA = 30°. Table 2 fully confirms that cycling corrodes indium from ITO showing a large decrease of the In/Sn ratio with cycling and a decrease, for the cycled sample, for TOA = 30°. Concerning the X/Si ratios, they strongly increase with cycling, denoting a strong loss of PDMS during cycling. However, the change in ratio with TOA shows that PDMS still remains in the sample, covering, at least partially, the HPW/PAH film.

For the as-deposited film ITO/PAH(HPW/PAH)$_5$, all the atomic ratios X/In are much lower than in the preceding film and rather independent of TOA. With cycling, they increase by about an order of magnitude but remain independent of TOA. These results are consistent with an important mixing of In with the film already during its building and an important loss of In^{3+} during cycling. Another hypothesis for explaining the large increase in X/In with cycling would be the change from an island-like structure, in the as-prepared film, to a film uniformly covering the substrate. However, in this case, the X/In ratios should display an important change with TOA, which is not the case. Once again, the In/Sn ratio may help to further clarify this question: In/Sn in the as-prepared film does not exhibit any change with TOA and presents the same value found in the film ITO/PDMS/PAH/(HPW/PAH)$_5$, which rules out the mixing of In^{3+} with the film. This mixing should have as consequence an increase of the In/Sn ratio, which is not verified. The cycled films present an overall decrease of the In/Sn ratio relatively to uncycled ones. However, contrarily to the uncycled films, the cycled ones present an In/Sn ratio increasing from TOA = 90° to TOA = 30°. One may therefore conclude that the as-prepared films are not dense and the substrate is easily accessible as observed by FEG-SEM. Cycling simultaneously induces film rearrangement, with a larger coverage of the substrate, and loss of In^{3+} from the substrate into the solution with some retention in the film. Substrate corrosion with indium diffusion through the film into the solution is also supported by the analysis of the charging accumulation correction, induced by photoelectron ejection, of the as-deposited film and after potential cycling. For the film on ITO pre-coated with just PAH, there is no shift in In $3d_{5/2}$ BE due to charging in the as-deposited sample, but it is around 1 eV in the cycled film, which is due to higher electrical resistance in the cycled electrode. This increase in surface resistivity can be assigned to a de-doping of the ITO semiconducting layer upon potential cycling in acidic solution.

The XPS region N 1s was fitted with 2 peaks 2.2 ± 0.4 eV apart for all films. They were centred at 402.6 ± 0.3 eV and 400.4 ± 0.4 eV for the as-prepared films and at 402.2 ± 0.2 eV and 399.7 ± 0.3 eV for the cycled films as shown in Fig. 6C and D respectively for the hybrid film with 5 bilayers of (HPW/PAH) pre coated with PDMS/PAH. Similar spectra for the hybrid film pre coated with PAH are shown in Fig. S9 in the ESI.† The peaks are assigned to the PAH nitrogen in protonated alkylamine (alkylammonium) and amine group, respectively. Nitrogen exists just in PAH. In the pristine polyelectrolyte (chlorine being the counterion), N 1s is centred at 401.46 eV.[51] The BE values for the protonated ammonium reported here are higher than the latter value because they tend to increase when PAH is mixed with other polyelectrolytes such as poly(styrene sulfonate), which would give 403.0 ± 0.2 eV.[64] In the same system, the component assigned to the primary alkylamine groups was found at 401.0 ± 0.2 eV. This shows that in PAH interacting with polyelectrolytes the nitrogen is involved in hydrogen bonding with the neighbourhood, thus increasing the N 1s BE. It should be noticed that we have exchanged the chloride ion by the phosphotungstate, thus the observed shift of the BE to higher values indicates supramolecular interaction of the $[PW_{12}O_{40}]^{3-}$ polyion with PAH. The BE shift to lower values after cycling is also an evidence for weaker supramolecular interactions of the reduced phosphotungstates. An additional feature of the N 1s region in Tables 1 and 2 is the higher deprotonation in the film without PDMS. Also, the angular analysis shows that the as-prepared films exhibit segregation of deprotonated nitrogen at the surface. The segregation in the cycled films also exists but it is much lower due to electrolyte diffusion through the film during cycling.

Summarizing, the potential cycling has a clear effect of homogenization of the film together with a migration toward the outer surface and loss of tungsten from the film.

C.2.5 Electrochemical behaviour of 5-bilayers (HPW/PAH) films on ITO/PDMS/PAH toward *s*-triazines detection. Fig. 7 shows the CVs for the film containing 5 bilayers of (HPW/PAH) on ITO/PDMS/PAH electrodes after 50 successive cycles of potential cycling in the absence and in the presence of atrazine (Fig. 7A) and of melamine (Fig. 7B). This previous procedure was necessary because after 50 successive cycles, the electrochemical properties of the film are constant. Independently of the triazines, the anodic current density increases with increasing triazine concentration, thus indicating electrooxidation of the triazines superimposed with the anodic processes for HPW. The bare electrode was also able to electrooxidize triazines, but at a more positive potential, around 150 mV *vs.* SCE, and lower current density than for the modified electrode in Fig. 7 as observed in Fig. S10 in the ESI.† This confirms electrocatalysis in the oxidation of triazines by the modified electrode. The ESI† also brings an explanation of this process with differential pulse voltammetry (DPV) studies of the modified electrode in the anodic region, in the absence and in the presence of triazines (Fig. S11 and S12†). In the presence of melamine, DPV for the modified electrode showed a new peak around 20 mV (*vs.* SCE), whose charge density increased linearly with increasing concentration of melamine between 4.0×10^{-8} mol L^{-1} and 9.0×10^{-8} mol L^{-1}. For atrazine measurements, the DPV experiments resemble those in the presence of melamine, thus a similar process must occur with the two *s*-triazines. However, the linear range for the response for electrooxidation of atrazine varied between 1.0×10^{-6} mol L^{-1} and 4.0×10^{-6} mol L^{-1} as shown in the inset. Thus, the hybrid films showed higher faradaic currents toward melamine than atrazine, even though there was no difference in electrooxidation potential between these triazines. Therefore, the films

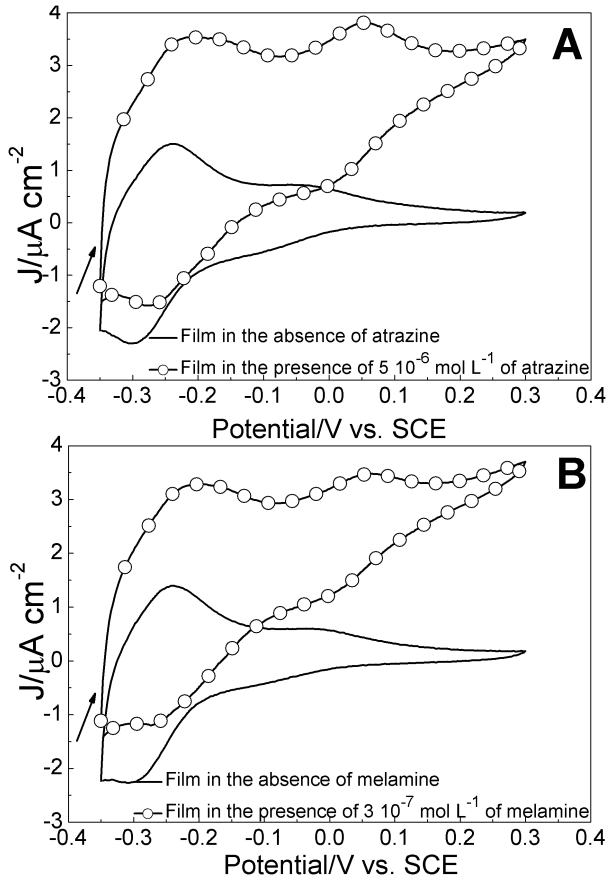

Fig. 7 CVs for a film containing 5 bilayers of (HPW/PAH) on ITO substrates pre-coated with (PDMS/PAH) in the absence (full line) and in the presence (-o-) of a (A) 5.0×10^{-6} mol L^{-1} atrazine solution; (B) 3.0×10^{-7} mol L^{-1} melamine solution. The supporting electrolyte was an aqueous solution of $HClO_4$ at pH = 1.0. Scan rate: 20 mV s^{-1}.

display similar thermodynamic reactivity but significant differences in their electron exchange rates.

The electrochemical detection of melamine and atrazine is normally made under neutral pH.[65–69] We therefore compare our results obtained under acidic conditions with those under similar experimental conditions. Recently, Xu *et al.* developed an electrochemical sensor to detect melamine with a thin film of molecularly imprinted sol–gel polymers fabricated on glassy carbon electrode by electropolymerization.[70] DPV experiments were performed using H_2SO_4 1 mol L^{-1} and KCl 0.1 mol L^{-1} as supporting electrolyte. Electrooxidation of melamine was monitored at +0.7 V *vs.* SCE with a linear range of concentration between 6.3×10^{-7} to 1.1×10^{-4} mol L^{-1}. There are two advantages in the electrode modified with 5-bilayers (HPW/PAH) used here to determine melamine, since both the applied potential and the dynamic range were lower than that reported by Xu *et al.*

With regard to atrazine detected in acidic medium, Pesavento *et al.*[71] produced an electrochemical sensor using glassy carbon or graphite electrodes with molecularly imprinted polymeric membranes. Amperometric experiments were carried out at −0.85 V *vs.* Ag/AgCl followed by a pulse at +0.5 V *vs.* Ag/AgCl in aqueous solution of Britton–Robinson buffer at pH 1.5. Svorc *et al.* performed electrochemical determination of atrazine using boron-doped diamond electrode and square wave voltammetry as technique.[72] Atrazine was electroreduced at −1.1 V *vs.* Ag/AgCl in Britton–Robinson buffer solution at pH 3.0 as supporting electrolyte. In both cases the detection potential is much higher than in our results, while the range of concentration is similar.

D Conclusion

In this paper, we exploited the capability of the LbL technique to control molecular architecture and produce hybrid films with HPW alternated with PAH, with optimized properties being reached when a PDMS layer was pre-deposited onto the ITO substrate. Since the film properties depend on various parameters, optimization of fabrication conditions was based on SPR and FT-IRRAS experiments. With this ITO/PDMS/PAH(HPW/PAH)$_5$ architecture, the best electrochemical response in acidic media was achieved because PDMS partially prevents HPW desorption. Such protection is only possible as PDMS molecules diffuse toward the outer layer in 5-bilayers (HPW/PAH) LbL films, which was confirmed with FT-IRRA spectroscopy, XPS and FEG-SEM measurements. We therefore used the (HPW/PAH) LbL films deposited onto a (PDMS/PAH) modified ITO to detect melamine and triazine, upon exploiting the electrooxidation of these *s*-triazines induced by the films. The kinetic reactivity is different for the *s*-triazines probably owing to reorganization energy, which led to distinct electron transfer rates between each triazine and HPW. Finally, the results presented here demonstrate that the control of the architecture of hybrid LbL films containing HPW could induce a promising environmental application such as the detection of s-triazine compounds.

Acknowledgements

This work was supported by FAPESP, CNPq, CAPES and Brazilian Network nBioNet.

References

1 G. Decher, *Science*, 1997, **277**, 1232.
2 W. B. Stockton and M. F. Rubner, *Macromolecules*, 1997, **30**, 2717.
3 Y. Shimazaki, M. Mitsuishi, S. Ito and M. Yamamoto, *Langmuir*, 1997, **13**, 1385.
4 P. Kohli and G. J. Blanchard, *Langmuir*, 2000, **16**, 8518.
5 J. Anzai and Y. Kobayashi, *Langmuir*, 2000, **16**, 2851–2856.
6 X. Shi, M. Shen and H. Mohwald, *Prog. Polym. Sci.*, 2004, **29**, 987.
7 V. Zucolotto, M. Ferreira, M. R. Cordeiro, C. J. L. Constantino, W. C. Moreira and O. N. Oliveira Jr, *Sens. Actuators, B*, 2006, **113**, 809.
8 N. Alexeyeva and K. Tammeveski, *Anal. Chim. Acta*, 2008, **618**, 140.

9 S. Liu, D. Volkmer and D. G. Kurth, *J. Cluster Sci.*, 2003, **14**, 405.
10 A. Kuhn, N. Mano and C. Vidal, *J. Electroanal. Chem.*, 1999, **462**, 187.
11 O. V. Cherstiouk, A. N. Simonov and G. A. Tsirlina, *Electrocatalysis*, 2012, **3**, 230.
12 M. Lu, D. Lee, W. Xue and T. Cui, *Sens. Actuators, A*, 2009, **150**, 280.
13 B. H. Han, I. Manners and M. A. Winnik, *Chem. Mater.*, 2005, **17**, 3160.
14 A. C. Perinotto, L. Caseli, C. O. Hayasaka, A. Riul Jr, O. N. Oliveira Jr and V. Zucolotto, *Thin Solid Films*, 2008, **516**, 9002.
15 M. L. Moraes, N. C. De Souza, C. O. Hayasaka, M. Ferreira, U. P. Rodrigues-Filho, A. Riul Jr, V. Zucolotto and O. N. Oliveira Jr, *Mater. Sci. Eng., C*, 2009, **29**, 442.
16 S. Liu, H. Mohwald, D. Volkmer and D. G. Kurth, *Langmuir*, 2006, **22**, 1949.
17 D. E. Katsoulis, *Chem. Rev.*, 1998, **98**, 359.
18 E. Papaconstantinuou, *Chem. Soc. Rev.*, 1989, **18**, 1.
19 M. N. Timofeeva, *Appl. Catal., A*, 2003, **256**, 19.
20 M. Sadakane and E. Steckhan, *Chem. Rev.*, 1998, **98**, 219.
21 T. Yamase, *Chem. Rev.*, 1998, **98**, 307.
22 M. de Oliveira Jr, A. Lopes de Souza, J. Schneider and U. Pereira Rodrigues-Filho, *Chem. Mater.*, 2011, **23**, 953.
23 E. P. Ferreira-Neto, F. L. S. de Carvalho, S. Ullah, V. C. Zoldan, A. A. Pasa, A. L. de Souza, L. C. Battirola, P. Rudolf, S. A. Bilmes and U. P. Rodrigues Filho, *J. Sol-Gel Sci. Technol.*, 2013, **66**, 363.
24 A. L. Souza, L. A. Marques, M. N. Eberlin, P. A. P. Nascente, P. S. P. Herrmann Jr, F. L. Leite and U. P. Rodrigues-Filho, *Thin Solid Films*, 2012, **520**, 3574.
25 S. Liu and Z. Tang, *Nano Today*, 2010, **5**, 267.
26 T. Dong, H. Ma, W. Zhang, L. Gong, F. Wang and C. Li, *J. Colloid Interface Sci.*, 2007, **311**, 523.
27 H. Ma, T. Dong, F. Wang, W. Zhang and B. Zhou, *Electrochim. Acta*, 2006, **51**, 4965.
28 L. Cheng and J. A. Cox, *Chem. Mater.*, 2002, **14**, 6.
29 Y. Gu, H. Ma, K. P. O'Halloran, S. Shi, Z. Zhang and X. Wang, *Electrochim. Acta*, 2009, **54**, 7194.
30 P. J. Kulesza, M. Chojak, K. Karnicka, K. Miecznikowski, B. Palys, A. Lewera and A. Wieckowski, *Chem. Mater.*, 2004, **16**, 4128.
31 A. Z. Ernst, S. Zoladek, K. Wiaderek, J. A. Cox, A. Kolary-Zurowska, K. Miecznikowski and P. J. Kulesza, *Electrochim. Acta*, 2008, **53**, 3924.
32 L. Sun, D. V. Ca and J. A. Cox, *J. Solid State Electrochem.*, 2005, **9**, 816.
33 S. Liu, D. G. Kurth, B. Bredenkotter and D. Volkmer, *J. Am. Chem. Soc.*, 2002, **124**, 12279.
34 L. Cheng and J. A. Cox, *Electrochem. Commun.*, 2001, **3**, 285.
35 Y. Feng, Z. Han, J. Peng, J. Lu, B. Xue, L. Li, H. Ma and E. Wang, *Mater. Lett.*, 2006, **60**, 1588.
36 B. Xu, L. Xu, G. Gao and Y. Jin, *Appl. Surf. Sci.*, 2007, **253**, 3190.
37 L. Cheng and S. Dong, *J. Electrochem. Soc.*, 2000, **147**, 606.
38 D. M. Fernandes, H. M. Carapuça, C. M. A. Brett and A. M. V. Cavaleiro, *Thin Solid Films*, 2010, **518**, 5881.
39 L. Cheng and S. Dong, *J. Electroanal. Chem.*, 2000, **481**, 168.
40 S. Liu, D. Volkmer and D. G. Kurth, *Anal. Chem.*, 2004, **76**, 4579.
41 M. Sosnowska, M. Goral-Kurbiel, M. Skunik-Nuckowska, R. Jurczakowski and P. J. Kulesza, *J. Solid State Electrochem.*, 2013, **17**, 1631.
42 B. Layla Mehdi, I. A. Rutkowska, P. J. Kulesza and J. A. Cox, *J. Solid State Electrochem.*, 2013, **17**, 1581.
43 K.-K. Shiu and F. C. Anson, *J. Electroanal. Chem.*, 1991, **309**, 115.
44 D. Martel and A. Kuhn, *Electrochim. Acta*, 2000, **45**, 1829.
45 Z. C. Y. Chan and W.-F. Lai, *Trends Food Sci. Technol.*, 2009, **20**, 366.
46 D. W. Gammon, C. N. Aldous, W. C. Carr Jr, J. R. Sanborn and K. F. Pfeifer, *Pest Manage. Sci.*, 2005, **61**, 331.
47 J. Yu, C. Zhang, P. Dai and S. Ge, *Anal. Chim. Acta*, 2009, **651**, 209.
48 R. Shoji, T. Takeuchi and I. Kubo, *Anal. Chem.*, 2003, **75**, 4882.
49 C. Donley, D. Dunphy, D. Paine, C. Carter, K. Nebesny, P. Lee, D. Alloway and N. R. Armstrong, *Langmuir*, 2002, **18**, 450.
50 D. T. Sawyer, A. Sobkowiak and J. L. Roberts Jr, in *Electrochemistry for Chemists*, John Wiley & Sons, New York, 2nd edn, 1995, ch. 3, pp. 68–78.
51 G. Beamson and D. Briggs, in *High Resolution of XPS of Organic Polymers: The Scienta ESCA 300 database*, John Wiley & Sons, Chichester, 1992.
52 M. T. Pope and G. M. Varga Jr, *Inorg. Chem.*, 1966, **5**, 1249.
53 B. Keita and L. Nadjo, *J. Electroanal. Chem.*, 1987, **227**, 77.
54 J. Stotter, Y. Show, S. Wang and G. Swain, *Chem. Mater.*, 2005, **17**, 4880.
55 M. Senthilkumar, J. Mathiyarasu, J. Joseph, K. L. N. Phani and V. Yegnaraman, *Mater. Chem. Phys.*, 2008, **108**, 403.
56 C. Vanleugenhague and M. Pourbaix, in *Atlas of electrochemical equilibra in aqueous solution*, ed. M. Pourbaix, Pergamon Press, Oxford, 1966, pp. 436–442.
57 E. Deltombe, N. De Zoubov, C. Vanleugenhague and M. Pourbaix, in *Atlas of electrochemical equilibra in aqueous solution*, ed. M. Pourbaix, Pergamon Press, Oxford, 1966, pp. 475–484.
58 M. T. Pope, in *Comprehensive Coordination Chemistry*, ed. G. Wilkinson, R. D. Gillard and J. A. McCleverty, Plenum Press, New York, 1987, vol. 3, p. 1039.
59 M. S. Akhtar, K. K. Cheralathan, J. M. Chun and O. B. Yang, *Electrochim. Acta*, 2008, **53**, 6623.
60 F. C. Oliveira, J. Schneider, A. Siervo, R. Landers, A. M. G. Plepis, J. J. Pireaux and U. P. Rodrigues-Filho, *Surf. Interface Anal.*, 2002, **34**, 580.
61 L. Zhang, Q. Jin, J. Huang, Y. Liu, L. Shan and X. Wang, *Appl. Surf. Sci.*, 2010, **256**, 5911.
62 *X-Ray Photoelectron Spectroscopy Database, Standard Database 20, Version 3.5*, National Institute of Standards and Technology NIST, http://srdata.nist.gov/xps/Version_his.aspx, accessed in January 2011.

63 C. Nunes de Carvalho, A. M. Botelho do Rego, A. Amaral, P. Brogueira and G. Lavareda, *Surf. Coat. Technol.*, 2000, **124**, 70.
64 J. M. C. Lourenço, P. A. Ribeiro, A. M. Botelho do Rego, F. M. Braz Fernandes, A. M. C. Moutinho and M. Raposo, *Langmuir*, 2004, **20**, 8103.
65 Y. T. Liu, J. Deng, X. L. Xiao, L. Ding, Y. L. Yuan, H. Li, X. T. Li, X. N. Yan and L. L. Wang, *Electrochim. Acta*, 2011, **56**, 4595.
66 C. W. Liao, Y.-R. Chen, J.-L. Chang and J.-M. Zen, *J. Agric. Food Chem.*, 2011, **59**, 9782.
67 H. Akter, A. A. Shaikh, T. R. Chowdhury, M. S. Rahmam, P. K. Bakshi and A. J. Saleh Ahammad, *ECS Electrochem. Lett.*, 2013, **2**(8), B13.
68 H. V. Tran, R. Yougnia, S. Reisberg, B. Piro, N. Serradji, T. D. Nguyen, L. D. Tran, C. Z. Dong and M. C. Pham, *Biosens. Bioelectron.*, 2012, **31**, 62.
69 P. Norouzi, B. Larijani, M. R. Ganjali and F. Faridbod, *Int. J. Electrochem. Sci.*, 2012, **7**, 10414.
70 G. Xu, H. Zhang, M. Zhong, T. Zhang, X. Lu and X. Kan, *J. Electroanal. Chem.*, 2014, **713**, 112.
71 M. Pesavento, G. D'Agostino, R. Biesuz and G. Alberti, *Electroanalysis*, 2009, **21**, 604.
72 L. Svorc, M. Rievaj and D. Bustin, *Sens. Actuators, B*, 2013, **181**, 294.